Stokes drag on a cylinder in axial motion

T. J. Ui, R. G. Hussey, and R. P. Roger

Citation: Physics of Fluids **27**, 787 (1984); doi: 10.1063/1.864706
View online: http://dx.doi.org/10.1063/1.864706
View Table of Contents: http://scitation.aip.org/content/aip/journal/pof1/27/4?ver=pdfcov
Published by the AIP Publishing

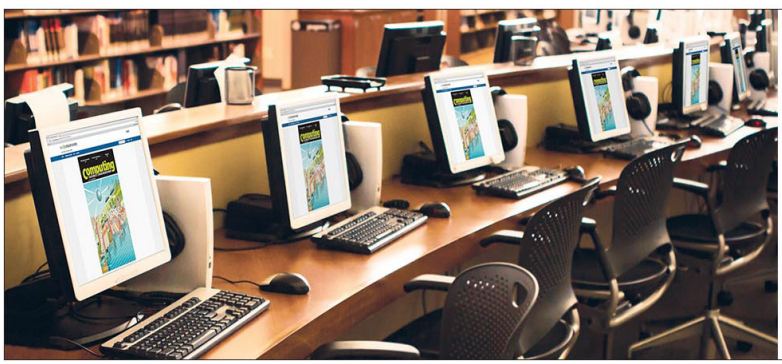

Stokes drag on a cylinder in axial motion

T. J. Ui and R. G. Hussey
Department of Physics and Astronomy, Louisiana State University, Baton Rouge, Louisiana 70803
R. P. Roger
Department of Chemistry and Physics, Northwestern State University, Natchitoches, Louisiana 71457

(Received 25 July 1983; accepted 11 January 1984)

Measurements are presented for the drag on a circular cylinder moving along its axis of rotational symmetry at low Reynolds number. The influence of an exterior cylindrical boundary is taken into account by making measurements with boundaries of different diameter and using an empirical correlation to extrapolate to infinite boundary diameter. The results for cylinders with length to diameter ratio (L/D) between 4 and 100 agree well with the calculated values of Youngren and Acrivos. The results for disks ($0.019 < L/D < 0.26$) are consistent with a linear interpolation between the value for a disk of zero thickness and the experimental points of Heiss and Coull. Beads-on-a-shell calculations are presented for both axial and transverse motion of cylinders with $0 \leqslant L/D \leqslant 10$. Interpolated values of the ratio of transverse to axial drag are used to obtain approximate values of transverse drag for $10 < L/D < 100$.

I. INTRODUCTION

A. Statement of the problem

Consider the drag on a circular cylinder moving parallel to its axis at low Reynolds number. The geometry and notation are given in Fig. 1: A Newtonian fluid of viscosity μ and density ρ is contained in a cylindrical tank of diameter H. A solid circular cylinder of length L and diameter D is coaxial with the outer boundary and is moving with constant velocity U along its axis. The midpoint of the cylinder is a distance S_b from the bottom of the tank and S_t from the top. The Reynolds number $UL\rho/\mu$ is presumed to be $\ll 1$. Solutions are available for several limiting cases of this problem.

B. Limiting cases

1. Cylinder of infinite length in a coaxial cylindrical boundary of infinite length ($S_t \to \infty$, $S_b \to \infty$, $L \to \infty$)

The solution for this case is given by Happel and Brenner,[1] but there is a typographical error in their expression. The correct expression is

$$F \equiv \frac{F'}{2\pi\mu U} = \frac{\sigma^2 - 3 + [4(\ln\sigma)/(\sigma^2 - 1)]}{[(\sigma^2 + 1)(\ln\sigma)] - 1}, \tag{1}$$

where F' is the drag per unit length and $\sigma = H/D$. For $\sigma \gg 1$, $F \to (\ln\sigma)^{-1}$, so for a fluid of infinite extent ($\sigma \to \infty$) the drag is zero, which means simply that the only steady flow solution is one for which the entire fluid is moving with velocity U. The same conclusion can be drawn from the solution for the impulsively started axial motion of an infinite cylinder in the limit of large time.[2]

2. Cylinder of finite length in a fluid of infinite extent ($S_t \to \infty$, $S_b \to \infty$, $H \to \infty$)

For the case $L \gg D$, several approximate solutions have been found. Burgers[3] represented the cylinder by a line of force along its axis and obtained for the dimensionless drag per unit length

$$F = \epsilon/(1 - 0.72\epsilon), \tag{2}$$

where $\epsilon = [\ln(2L/D)]^{-1}$. Broersma[4] used a similar approach and obtained a numerical coefficient of 0.81 instead of 0.72. Cox[5] showed that the coefficient should be $\alpha \equiv \frac{1}{2} - \ln 2 \simeq 0.806\,85$. Batchelor[6] derived results for the axial and transverse drag on slender bodies of arbitrary cross-sectional shape. When restricted to the case of a circular cylinder in axial motion, his result for the dimensionless drag per unit length is

$$F_B = \epsilon(1 - H_{01})/(1 - \tfrac{1}{2}\epsilon) + \epsilon^3(H_{02} - \tfrac{1}{2}H_{01}) \simeq \epsilon + 0.806\,85\epsilon^2 + 0.828\,54\epsilon^3, \tag{3}$$

where $H_{01} = -1 + \ln 2$ and $H_{02} = 1 + (1 - \ln 2)^2$

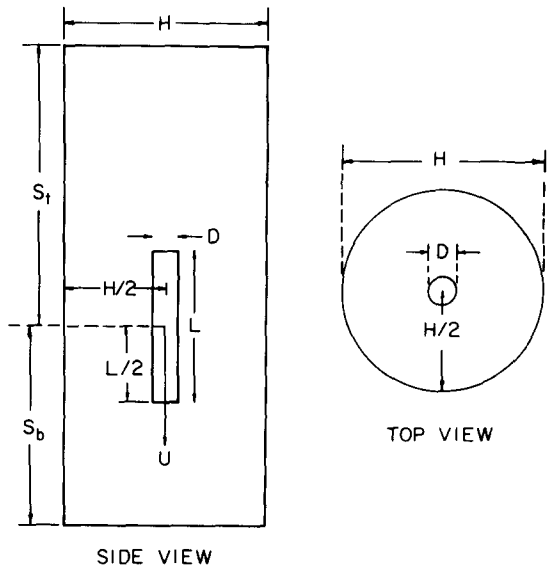

FIG. 1. Geometry and notation for a circular cylinder of finite length moving axially through a viscous fluid bounded by a cylindrical container.

 0031-9171/84/040787-09$01.90

$-(\pi^2/12)$. Keller and Rubinow[7] used the method of matched asymptotic expansions to obtain

$$F_{KR} = \epsilon/(1 - \alpha\epsilon - \beta\epsilon^2), \tag{4}$$

where $\beta = 1 - (\pi^2/12)$. When written as a series in increasing powers of ϵ, Keller and Rubinow's result is the same as that of Batchelor for terms up to ϵ^3. Russel *et al.*[8] used numerical integration of the slender body integral equations to obtain a more accurate solution. From their Fig. 3 we have obtained the following approximate result:

$$F_R = F_{KR} + 4\epsilon^5 + 28\epsilon^6, \tag{5}$$

which represents their results well for $\epsilon < 0.275$.

For $0.25 \leqslant L/D \leqslant 4$, values of the drag have been calculated by Youngren and Acrivos,[9] Gluckman *et al.*,[10] and Swanson *et al.*[11] Youngren and Acrivos used a surface distribution of point forces and numerical integration over elements of surface area. Gluckman *et al.* approximated the cylinder by a set of touching oblate spheroids. Swanson *et al.* used the beads-on-a-shell model. The results of these three approaches are in substantial agreement and also agree well with the experimental values of Heiss and Coull[12] and of Blumberg and Mohr.[13] In the limit $L/D \to 0$, the drag should approach the well-known solution for a disk of zero thickness, $8\mu UD$.

Youngren and Acrivos also calculated the drag in the intermediate range $4 \leqslant L/D \leqslant 100$. Their values for L/D equal to 60, 80, and 100 are in good agreement with the slender body results of Russel *et al.* Gluckman *et al.* obtained approximate values of the drag for L/D equal to 10, 20, and 40 by representing the cylinder by touching prolate spheroids; their values are consistently lower than those of Youngren and Acrivos. De Mestre[14] has made measurements for L/D ranging from 15.6 to 98.1. His experimental values of drag are 13% to 24% higher than his slender body calculations, which include the effects of parallel plane walls.

3. Cylinder of finite length approaching an infinite plane wall ($S_t \to \infty$, $H \to \infty$)

The case of a slender cylinder ($L \gg D$) has been treated by de Mestre and Russel.[15] Their result is

$$F = \epsilon[1 + \tfrac{1}{2}\epsilon(W - 0.614)], \tag{6}$$

where $W = \frac{1}{2}\gamma + (\gamma^{-1} + 1)\ln(1 + \gamma) + (\gamma^{-1} - 1)\ln(1 - \gamma)$ and $\gamma = \frac{1}{2}L/S_b$. For $\gamma \ll 1$, $W \simeq 3\gamma/2$. When the cylinder is far from the wall ($W \to 0$), Eq. (6) does not agree with Eqs. (3) and (4) beyond the first order in ϵ.

The case of a thin disk close to the bottom wall ($L \ll D$, $S_b - \frac{1}{2}L \ll D$) has been treated by means of lubrication theory[16] and is a particular case of the squeeze film problem.

C. The present work

We report here measurements of the drag on cylinders with L/D ranging from 4 to 230 and the drag on disks with L/D ranging from 0.25 to 0.019. The influence of the top and bottom boundaries is assumed to be negligible and the effect of the cylindrical sidewall is taken into account by an empirical correlation. We present also beads-on-a-shell calculations of the drag for $0 < L/D \leqslant 10$.

II. METHODS AND MATERIALS

A. Experiment

Measurements were made of the terminal velocity of a disk or a long cylinder falling in a silicone liquid. For the measurements on disks, the release mechanism, the liquid, the container, and the measuring techniques were the same as those described by Amarakoon.[17] For the measurements on cylinders, a slightly larger container was used, of square cross section (30.48 cm × 30.48 cm), and the fluid depth was 49 cm. Outer boundaries of circular cross section (ranging from 2.18 to 23.6 cm i.d.) were obtained by using the same six glass and plastic tubes employed by Amarakoon.

Twenty-eight steel and four acrylic rods were used for the long cylinders. The steel cylinders ranged in length from 0.384 to 10.98 cm and in diameter from 0.0396 to 0.0987 cm, with $4.21 < L/D < 231$, while the acrylic cylinders were all cut from the same rod of diameter 0.338 cm, with $3.74 < L/D < 9.37$. The cylinders were released from rest by hand. A vertical orientation was obtained by releasing them through a vertical hole in an acrylic block (2.4 cm thick) at the top of the tank. The terminal velocity of a cylinder was obtained by measuring the time of passage between two marks on the side of the tank. The marks were 5, 10, or 20 cm apart and were located in the middle portion of the tank. Times were determined by manual operation of a stopclock (Standard Electric model S-10) having a precision of 0.01 sec.

The liquid used for the long cylinders had a nominal kinematic viscosity of 36 cm^2/sec. It was obtained by mixing 10 cm^2/sec liquid (approximately 48% by volume) with 125 cm^2/sec liquid. The viscosity, measured with a Cannon Ubbelohde capillary viscometer, was observed to increase slowly with time in a manner similar to that reported by Amarakoon.[17] The approach to a steady value was approximately exponential, with an e-folding time of 1 month for the present liquid compared to a time of 7 months for Amarakoon's liquid. The more rapid approach to a steady value for the present liquid was achieved by pouring the liquids into the tank alternately in thin layers rather than adding one liquid in bulk to the other before stirring.

The influence of fluid inertia and the effect of the top and bottom boundaries were assumed to be negligible. These assumptions were checked in the following manner: The inertial contribution to the drag was estimated from Breach's theory[18] for spheroids. For the long cylinders, approximated by prolate spheroids, this contribution did not exceed 0.3% and was typically less than 0.1%. For the disks, approximated by oblate spheroids, the largest contribution was 0.62% and the typical value was 0.3%. The effects of the free surface at the top and the solid wall at the bottom were checked in two ways: (1) by measuring cylinder velocities at different depths with a constant overall depth of 49 cm, and (2) by measuring the velocity of a cylinder at the middle of the tank with two different fluid depths, 46 cm and 16.6 cm. As long as the lower end of the cylinder was more than one cylinder length from the bottom, the velocity was the same within 0.4%. When a cylinder of length 4.2 cm was observed with the two different fluid depths, its velocity midway between the top and bottom of the tank was the same within 0.23%.

B. Calculations

The beads-on-a-shell method was used to calculate the drag on cylinders with $0.026 < L/D < 10$. In this method the cylinder is represented by an array of small spheres covering the surface of the cylinder. The drag on the array is determined by means of the modified Oseen interaction tensor. Several arrays of successively smaller spheres are used, with the ratio of sphere radius to cylinder radius ranging from 0.1 to 0.01. The drag on the cylinder is then obtained by extrapolating these values to zero sphere size. The computation required inversion of matrices ranging from 10×10 to 4200×4200. The majority of the calculations were performed on an IBM 370/3033 computer utilizing matrix inversion subroutines from the IMSL Library of Fortran Subroutines in Mathematics and Statistics (IMSL, Inc., Houston, Texas 77036). For the larger arrays the Gauss–Seidel iterative method was used. The iterative method was also used for a few of the smaller arrays, the computation of which was performed on an Olivetti M20 microcomputer.

The bead arrays used for the flat faces of the cylinder were similar to those employed previously for the disk of zero thickness.[19] The cylindrical surface was modeled both by stacking rings of beads directly on top of each other as well as by adjusting the orientation of successive rings of beads to hexagonally close-pack the beads on the side; the drag was the same for both models. For translation parallel to the cylinder axis the net drag on each array was determined by computing the force on a bead in each ring of the array, multiplying by the number of beads in the ring, and summing over all rings. This required inverting an $NR\times NR$ matrix, NR being the number of rings in that particular array. For translation perpendicular to the cylinder axis the net drag for each array was determined by computing the force on one-eighth of the array and multiplying by eight. This required inverting an $N/8\times N/8$ matrix, N being the total number of beads in that array. More details and references are given in an earlier paper[19] and in review articles by Teller *et al.*[20] and by Garcia de la Torre and Bloomfield.[21]

III. RESULTS

A. Long cylinders

The most difficult part in the experimental determination of the Stokes drag on an object is the proper assessment of the boundary effect. There are several theoretical treatments that can be used for guidance. Chang[22] derived an expression for the motion of an axisymmetric object along the axis of a circular cylindrical boundary. His result, applied to the present case, can be written in the form

$$F/F_\infty = 1 + (CF_\infty L/H), \tag{7}$$

where F_∞ is the dimensionless Stokes drag (made dimensionless by the factor $2\pi\mu UL$) in a fluid extending to infinity and $C = 1.403$. Brenner[23] has obtained a more general result for nonaxisymmetric particles and for outer boundaries of arbitrary shape. The coefficient in Brenner's theory corresponding to C in Eq. (7) depends on the shape of the outer boundary but not on the shape of the particle. Wakiya[24] has found the effect of a cylindrical outer boundary on the drag of a spheroid, including terms up to $(L/H)^3$. In the limit $L \ll H$ the results of Chang, Brenner, and Wakiya are identical when the outer boundary is cylindrical.

In the present case (a long cylinder moving lengthwise along the axis of a cylindrical boundary) we have observed that the dimensionless drag ($F = \text{drag}/2\pi\mu UL$) is a linear function of the inverse of the boundary diameter ($1/H$). This linear relation, shown in Fig. 2, suggests that a linear extrapolation ($1/H \to 0$) will give the Stokes drag for a fluid of infinite extent. Such an extrapolation procedure is supported by the result of Wakiya[24] (shown as the dashed lines in Fig. 2) for a long prolate spheroid. One can see from Fig. 2 that as the length to diameter ratio increases, the observed behavior of the cylinder more closely approaches the theoretical result for the spheroid, as one would expect. Our measured values can be written in the form of Eq. (7) but the coefficient C was found to depend weakly on L/D and to approach the value 1.403 from above as L/D increases. The final result is

$$(F/F_\infty) - 1 = CF_\infty L/H,$$
$$C = \begin{cases} 1.60 \pm 0.15, & \text{for } L/D < 40, \\ 1.403 + (7D/L), & \text{for } L/D > 40. \end{cases} \tag{8}$$

Figure 3 shows our data for long cylinders and indicates that Eq. (8) is valid for $L/H < 1.2$.

The theoretical treatments of Brenner[23] and Williams[25] for the influence of a boundary on the drag of a particle indicate that the correct expression in that case is

$$F/F_\infty = [1 - (CF_\infty L/H) + O(L/H)^3]^{-1}, \tag{9}$$

which implies that a plot of $1/F$ vs $1/H$ should be linear over a wider range of H than a plot of F vs $1/H$. Our data indicate that the reverse is the case for a long cylinder moving axially, i.e., an expression in the form of Eq. (7) is more appropriate than an expression in the form of Eq. (9). The same conclusion can be drawn from Wakiya's theory for spheroids: the boundary effect for an oblate spheroid (moving along its minor axis) is more linear when $1/F$ is plotted versus $1/H$, but for a long prolate spheroid (moving along its major axis) it is

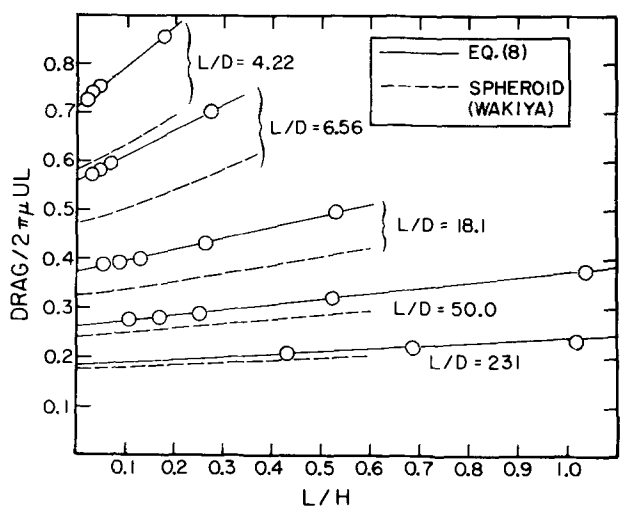

FIG. 2. The boundary effect for long cylinders. The solid lines represent our empirical correlation, Eq. (8), and the dashed curves represent results derived by Wakiya (Ref. 24) for the corresponding inscribed prolate spheroids.

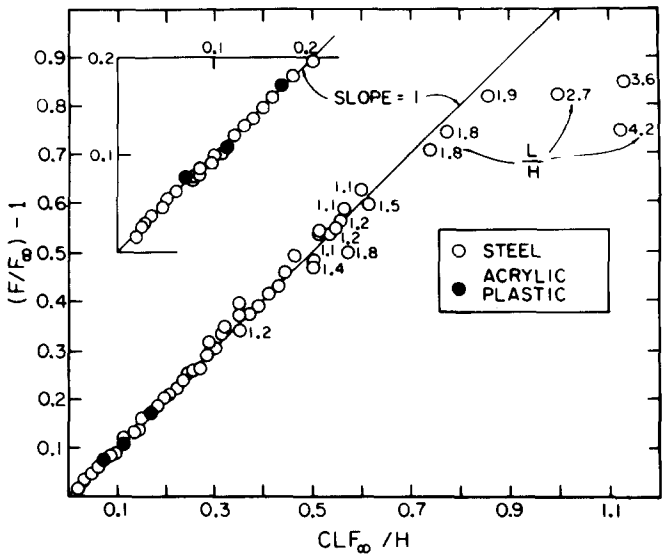

FIG. 3. Correlation of the boundary effect data for long cylinders. Values of L/H are given beside those points for which $L/H > 1.1$.

more linear when F is plotted versus $1/H$, as shown in our Fig. 2. The theory of Williams[25] indicates that it is not the boundary radius $H/2$ that should be used in Eq. (9) but rather the minimum distance from the body to the boundary. However, the difference between H and $H - D$ is insignificant for the long–thin cylinders.

The values of F obtained by extrapolation are compared with theory in Fig. 4. The theoretical results for slender cylinders, Eqs. (2)–(5), all have as the leading term $\epsilon = [\ln(2L/D)]^{-1}$, so a sensitive method of presenting the results is to plot $(F_\infty/\epsilon) - 1$ vs ϵ. As shown in the figure, our experimental values are in good agreement with the slender body results of Batchelor and of Russel *et al.* for $\epsilon < 0.2$, and agree well with the values calculated by Youngren and Acrivos for $4 \leqslant L/D \leqslant 100$. From the values of Youngren and Acrivos and from our own calculated values determined for $L/D = 10$ and 4, we have obtained the following empirical relation:

$$F = 0.0244 + 0.5504\epsilon + 3.328\epsilon^2 - 2.971\epsilon^3. \quad (10)$$

This relation is plotted as the dashed curve in Fig. 4. The

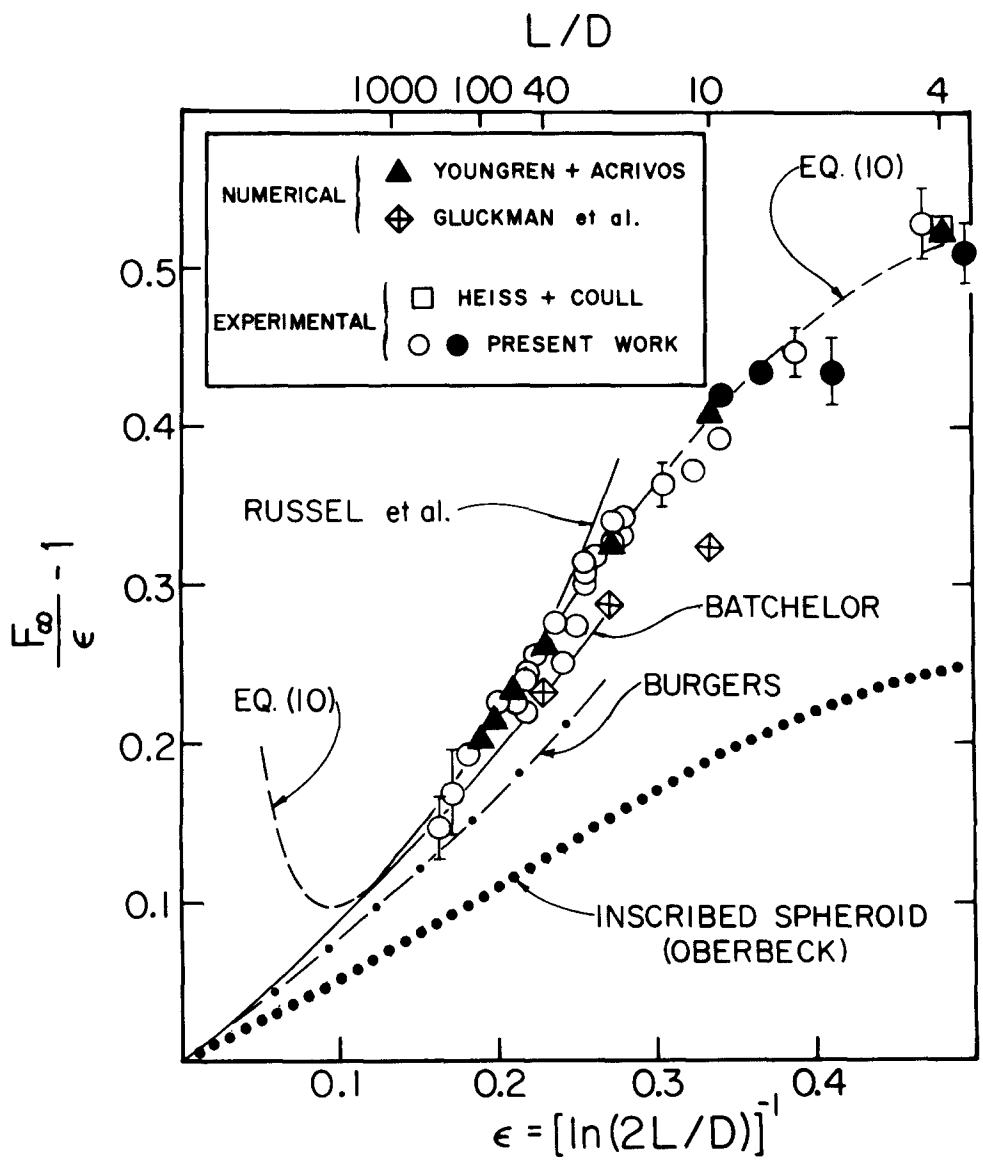

FIG. 4. Comparison of our experimental results for long cylinders with expressions from slender body theory and with numerical calculations. The open circles are our results for steel cylinders and the closed circles are for acrylic cylinders. Error bars are indicated for some selected experimental points.

result for the drag on an inscribed prolate spheroid, calculated from the exact solution of Oberbeck,[26] is similar in form to but consistently less than the drag on the corresponding circular cylinder.

B. Short cylinders

Values of the drag were calculated by means of the beads-on-a-shell method for cylinders of length to diameter ratio from 0 to 10. The results for both axial and transverse motion are presented in Table I, along with the calculated values of Youngren and Acrivos,[9] Gluckman *et al.*,[10] and Swanson *et al.*,[11] and the experimental values of Heiss and Coull.[12] Our values for the axial drag are consistent with but slightly lower than previous values. Here F_d is the axial drag divided by $8\mu UD$, the exact solution for the disk of zero thickness. The relation between F_d and the settling factor K (used by other authors) is

$$F_d = (3\pi/8K)(3L/2D)^{1/3}. \tag{11}$$

The quantity K is defined as $6\pi\mu UR$ divided by the drag, where R is radius of the sphere having a volume equal to the volume of the cylinder. For $L/D \leqslant 1$, our calculated values are represented well by the equation

$$F_d = 1 + 0.437A - 0.0749A^3 + 0.0623A^5 - 0.0250A^7, \tag{12}$$

where $A = L/D$.

Equation (12) is plotted in Fig. 5 along with our experimental results and the experimental results of Heiss and Coull[12] and of Blumberg and Mohr.[13] Also shown is Eq. (10), the curve fit for long cylinders. Neither Eq. (10) nor Eq. (12) represents the results well in the region $1 < L/D < 4$. The following equation serves as an interpolation between Eqs. (10) and (12) in that region:

$$F_d = 1.0276 + 0.3963A - 0.0259A^2 + 0.0014A^3. \tag{13}$$

Experimental values for the drag on the disks are shown as the open circles in Fig. 5. The disks were made from aluminum or acrylic plastic and ranged in diameter from 1.0 to 2.7 cm and in thickness from 0.052 to 0.30 cm. The influence of the outer boundary was determined as for long cylinders by using Wakiya's theory[24] for spheroids as a model. Wakiya's expression for the effect of a cylindrical boundary on the drag of an oblate spheroid can be written

$$F/F_\infty = [1 - \lambda(D/H) + \delta(D/H)^3]^{-1}, \tag{14}$$

where λ and δ are functions of the aspect ratio $A = L/D$. We assume that the boundary effect for disks can be represented by an expression having the same form as Eq. (14) but with different coefficients λ and δ. However, in the limit $A \to 0$, the value of λ must approach 1.786 and the value δ must approach 1.128 since in that limit both the oblate spheroid and the disk approach the same shape, namely the disk of zero thickness.

Empirical expressions for λ and δ were obtained as follows: Initial values for the drag F_∞ in a fluid of infinite extent were obtained by plotting $1/F$ vs $1/H$ and extrapolating to $(1/H) = 0$. These initial values were used along with data for which the cubic term in Eq. (14) could be neglected ($D/H < 0.15$) to determine the dependence of λ on A, which was found to be

$$\lambda = 1.786(1 + 0.44A). \tag{15}$$

TABLE I. Values of the dimensionless drag for short cylinders.

A. Axial motion

L/D	$F_d = \text{drag}/8\mu UD$				
	Present results	Youngren and Acrivos[a]	Gluckman *et al.*[b]	Swanson *et al.*[c]	Heiss and Coull[d]
0.00	1.0000				
0.25	1.1081				
0.50	1.2109	1.226	1.220	1.223	1.239
0.75	1.3076				
1.00	1.3994	1.414	1.405	1.409	1.408
1.50	1.5699				
2.00	1.7279	1.739	1.723	1.736	1.743
4.00	2.2881	2.297	2.270	2.294	2.304
10.00	3.6789	3.687			

B. Transverse motion

L/D	$\text{drag}/(16\mu UD/3)$			
	Present results	Swanson *et al.*[c]	Heiss and Coull[d]	
0.00	1.0001			
0.50	1.6606	1.663	1.671	
1.00	2.1243	2.126	2.141	
1.50	2.5319			
2.00	2.9094	2.908	2.903	
4.00	4.2518	4.239	4.236	
10.00	7.6240			

[a] Ref. 9.
[b] Ref. 10.
[c] Ref. 11.
[d] Ref. 12.

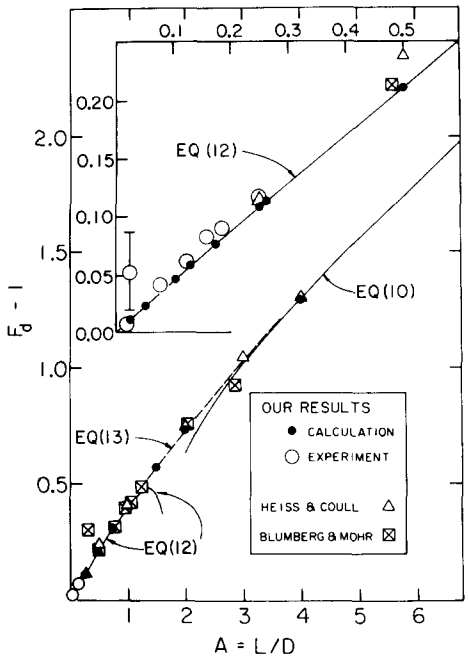

FIG. 5. Comparison of experimental results for short cylinders with our beads-on-a-shell calculations (small closed circles). Equations (10), (12), and (13) are empirical curve fits.

Equation (15) is consistent with Brenner's theory[23] for the boundary effect on a particle of arbitrary shape and our Eq. (12) for the dependence of F_∞ on A. Equation (15) was used along with data for which $D/H < 0.15$ to obtain secondary values of F_∞, which were then used along with Eq. (15) and all of the data ($0.043 < D/H < 0.31$) to obtain the following approximate expression for δ:

$$\delta = 1.128 + 3(A)^{1/2}. \tag{16}$$

Then Eqs. (15) and (16) were used to obtain the final values of F_∞. The resulting correlation of the boundary effect data for disks is shown in Fig. 6.

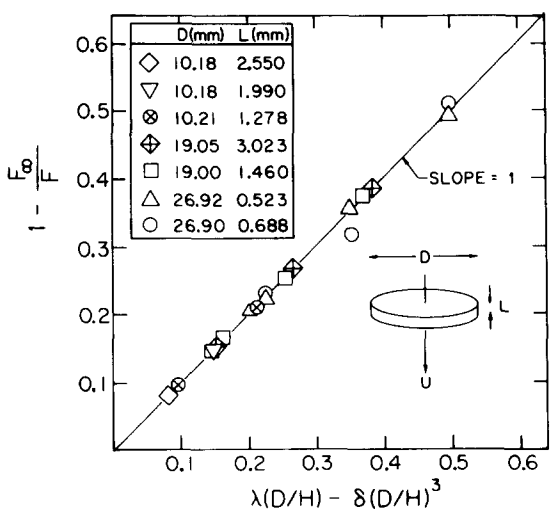

FIG. 6. Correlation of the boundary effect data for disks. The coefficients λ and δ are given by Eqs. (15) and (16), respectively. Both F and F_∞ are made dimensionless by the same factor, $8\mu UD$.

IV. DISCUSSION

The present measurements, combined with those of Heiss and Coull and Blumberg and Mohr, provide experimental values of the Stokes drag on a circular cylinder in axial motion for length to diameter ratios in the range 0.019 to 231. Over the entire range there is good agreement with the available theoretical results. Measurements are difficult for $L/D > 200$, but this is the region for which the slender body expressions [Eqs. (3)–(5)] are expected to be accurate. Similarly, for $L/D < 0.019$ it is reasonable to assume that the simple linear relation $8\mu UD\ [1 + 0.437\ (L/D)]$, obtained from the beads-on-a-shell calculations, will be valid. Therefore we conclude that accurate values of the Stokes drag for a cylinder in axial motion are available for all length to diameter ratios. Values of the drag can be obtained from Eq. (5) for $L/D > 75$, Eq. (10) for $4 < L/D < 75$, Eq. (13) for $1 < L/D < 4$, and Eq. (12) for $L/D < 1$.

For a cylinder moving in a direction perpendicular to its axis of rotational symmetry (transverse motion), accurate drag results are lacking in the intermediate region $10 < L/D < 100$. However, such results can be inferred by interpolation in the following manner: As $\epsilon \to 0$, the ratio of transverse drag (F_{tr}) to axial drag (F_{ax}) approaches 2, as pointed out by Taylor.[27] Tillett[28] and Weinberger[29] have shown that this limit is approached from below, i.e., $F_{tr}/F_{ax} < 2$ for $\epsilon > 0$. For $0 < \epsilon < 0.2$, values of the drag ratio F_{tr}/F_{ax} can be obtained from the slender body calculations of Russel *et al.*, as represented by our Eq. (5) and Stalnaker's[30] Eq. (4). At the other extreme ($\epsilon > 0.3$), values of F_{tr} and F_{ax} are available from our beads-on-a-shell calculations and from the measurements of Heiss and Coull. The resulting values of F_{tr}/F_{ax} are plotted versus ϵ in Fig. 7. Assuming that there is a smooth variation of the drag ratio in the intermediate re-

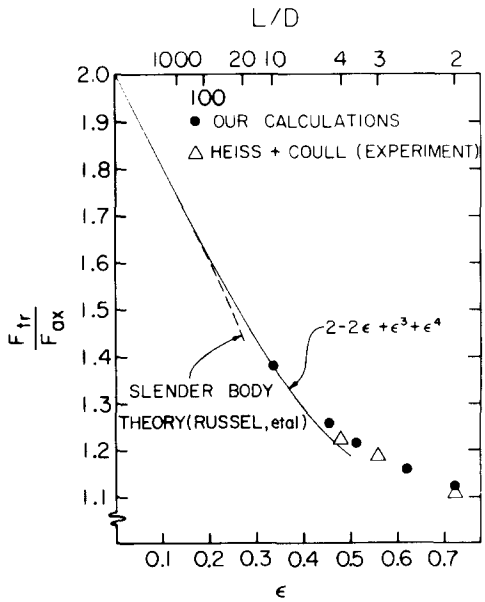

FIG. 7. Interpolation curve for the ratio of transverse to axial Stokes drag for a circular cylinder.

TABLE II. Values of F_{tr} obtained from the interpolated values of F_{tr}/F_{ax} (Fig. 7) combined with the values for F_{ax} from Youngren and Acrivos.

L/D	F_{tr}/F_{ax}	$F_{tr} = \text{drag}/2\pi\mu UL$
20	1.483	0.533
40	1.558	0.449
60	1.593	0.410
80	1.615	0.386
100	1.631	0.370

gion, we have found that the following simple equation can be used for interpolation:

$$F_{tr}/F_{ax} = 2 - 2\epsilon + \epsilon^3 + \epsilon^4. \tag{17}$$

From Eq. (17) and the values of F_{ax} calculated by Youngren and Acrivos it is possible to obtain the corresponding values of F_{tr}, which are given in Table II. Both F_{tr} and F_{ax} are made dimensionless by the same factor $2\pi\mu UL$, so for $\epsilon \ll 1$, F_{ax} approaches ϵ and F_{tr} approaches 2ϵ.

In Table I it is shown that our calculated values for the drag on short cylinders are slightly less than values calculated by other authors. We believe that these small differences are due to the manner in which the different calculations treat the sharp corners at which the curved cylindrical surface meets the flat end faces of the cylinder. Youngren and Acrivos have shown that the viscous stress at the surface is sharply peaked at the corner, as one would expect on physical grounds. We have obtained a similar result, as shown in Fig. 8. Here the normalized stress force (in the axial direction) is plotted for a cylinder of $L/D = 1$ as one proceeds

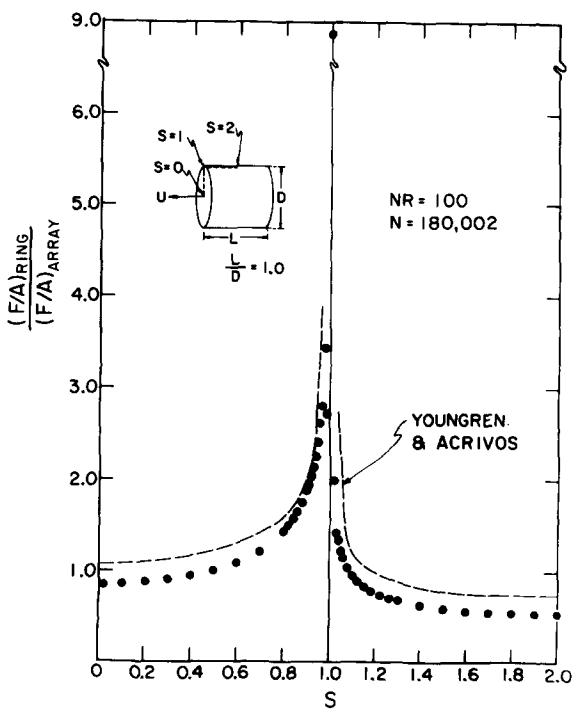

FIG. 8. Variation of the axial stress force with position on the cylinder. N is the total number of beads and NR is the number of rings of beads.

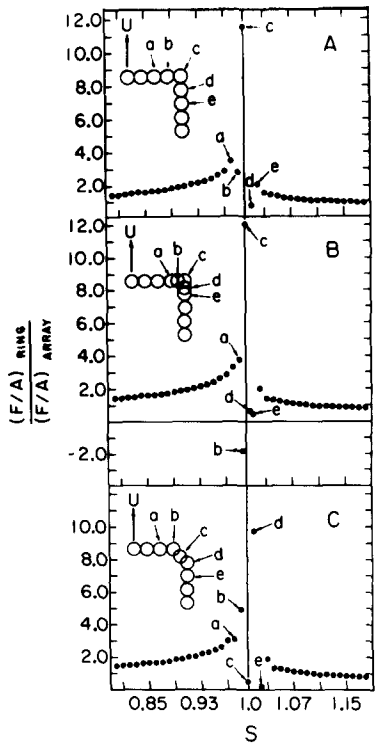

FIG. 9. Variation of the axial stress force near the corner for three different arrays of beads.

from the center of an end face ($S = 0$) around the corner ($S = 1$) to a point halfway up the cylindrical surface ($S = 2$), as done by Youngren and Acrivos. The normalized stress force is obtained by calculating the force on a particular axisymmetric ring of beads divided by the total surface area of the beads in that ring $[(F/A)_{\text{RING}}]$ and dividing that ratio by the ratio of the force on the entire array of beads to the surface area of the entire array $[(F/A)_{\text{ARRAY}}]$.

Figure 9 shows the changes that occur in the stress distribution near the corner when different arrays of beads are used. In an array of equally spaced beads (array A) with one bead (bead c) centered at the corner, the maximum stress force occurs on the bead at the corner, while the stress force on the two beads adjacent to the corner (beads b and d) is significantly lower than on other beads nearby. This peculiar drop in the stress on those beads immediately adjacent to the corner occurs regardless of the size of the beads, so it must be an artifact of the model rather than a real physical effect. When the corner is rounded (array C) by moving bead c to a position midway between beads b and d, the maximum stress force shifts to bead d (the bead nearest the corner on the cylindrical surface) while the stress force on beads c and e drops to a low value. In array B, the corner is square and additional overlapping beads are concentrated near the corner; again, the bead at the corner has the largest stress force, but now the overlapping bead b on the flat face has a negative value of stress force, and both beads d and e on the cylindrical surface have low values.

In Fig. 10 is shown the extrapolation of the drag to zero bead radius for each of the arrays in Fig. 9. The extrapolation curves for arrays A and B are practically identical, as are the extrapolated values of the drag F_d (1.2109 for both A and B).

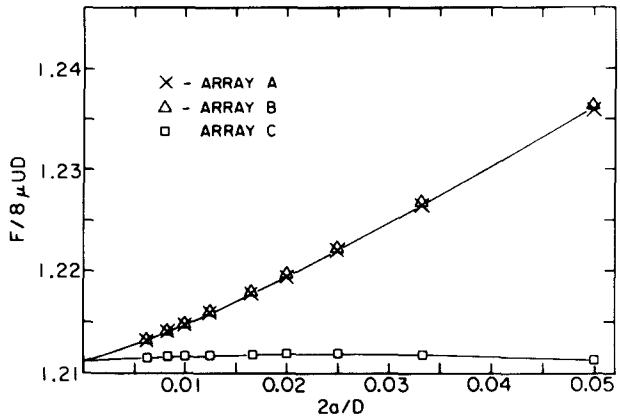

FIG. 10. Extrapolation curves for the three different arrays of Fig. 9.

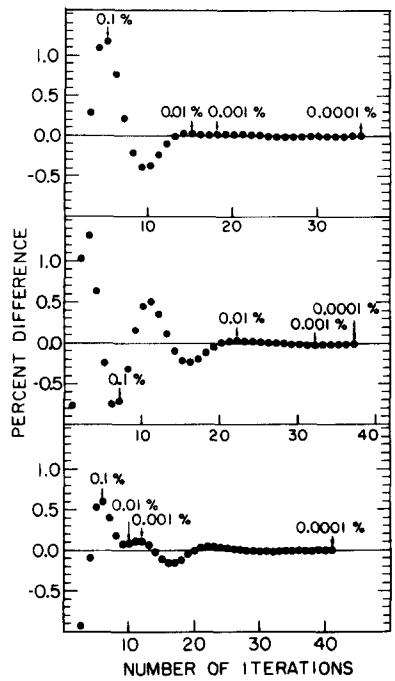

FIG. 11. Convergence of the Gauss–Seidel iteration for the case $L/D = 1$. The middle pattern was obtained when the initial estimate of the drag on each bead was taken as the total drag divided by the total number of beads. In the upper pattern, the initial estimate was 30% lower and in the lower pattern it was 30% higher. The arrows indicate points at which successive iterations differ by less than the given percentages.

For array C, although the extrapolation curve is considerably different, the extrapolated drag value $F_d = 1.2111$ is within 0.02% of the values for A and B. O'Brien[31] has pointed out that the infinite values of pressure that occur at sharp corners are mathematical rather than physical anomalies; every corner of a real object will be slightly rounded. Our results are consistent with those she has obtained by finite difference methods: when the corner point is part of the fluid rather than part of the solid surface (array C), the drag for nonzero sphere size is a better approximation to the extrapolated value.

The peculiar oscillation of the stress force near the corner suggests a possible flaw in the beads-on-a-shell method when applied to objects with sharp edges. To investigate this question further, we have used the method to calculate the drag on several objects for which analytical solutions are known. Wakiya[32] has recently developed from the original solution of Payne and Pell[33] explicit numerical values for the drag on a body consisting of the intersection of two spheres. From among his solutions we have chosen two symmetric double-convex lens shapes, one a thin lens in which the interior angle at the intersection of the two spherical surfaces is 30° and the other a thick lens in which the angle is 120°. The results of our calculations are given in Table III, which also includes our previous result for the disk of zero thickness[19] and new results for the sphere and the body of revolution whose section is a cardioid.[34] In each case the calculations were carried out until the ratio of bead diameter to outside diameter of the object was 0.015 or less, and extrapolation to zero bead diameter was done by least squares fit to a polynomial of order 1 to 3. For the two lens shapes and the flat disk, oscillations in the stress force occur which are similar to that of Fig. 9 (part A) but which are symmetrical about the edge. However, the amplitude of the oscillation decreases as the lens interior angle increases from 0° to 120°. As shown in the table, the differences between the calculated and the exact values for the drag are quite small. Therefore, we conclude that although the beads-on-a-shell method may give unrealistic oscillations in the stress force as a sharp corner is approached, the drag values obtained from the method are reliable, at least for the convex shapes to which it has been applied thus far. It should be pointed out, however, that these shapes do not include any for which separation occurs.[35]

TABLE III. Comparison between drag values calculated with the beads-on-a-shell method and exact solutions.

Shape	$F_d = \text{drag}/8\mu UD$		
	Calculated	Exact	% difference
disk	1.000 01	1.000 00	0.001
30° lens	1.000 21	1.000 32	0.012
120° lens	1.037 31	1.037 91	0.057
sphere	1.178 12	1.178 10	0.002
cardioid	1.161 40	1.161 55	0.013

There is an apparent inconsistency between our calculations for the short cylinders and the results obtained by Swanson *et al.*,[11] who also used the beads-on-a-shell method. We believe that the difference is due to the use of different cutoff values for the Gauss–Seidel iteration and the use of different extrapolation methods. Swanson *et al.* stopped their iteration when successive values differed by less than 0.1%, and they used a linear extrapolation to zero bead size. We have continued the iteration until successive values differed by less than 0.0001% and have extrapolated with least squares curve fits up to order 3. The convergence of the Gauss–Seidel iteration is illustrated in Fig. 11 for the case $L/D = 1.0$, total number of beads = 1202, and a ratio of bead diameter to cylinder diameter of 0.05. In using the Gauss–Seidel method it is necessary to make an initial estimate of the drag on each bead. When the average drag per bead for

the array was taken as the initial estimate (with each bead initially having equal drag), the convergence pattern shown in the middle of Fig. 11 was obtained. In the upper pattern the initial estimate was 30% lower than the average drag per bead and in the lower pattern the initial estimate was 30% higher. The arrows show the points at which successive values differ by less than 0.1%, 0.01%, 0.001%, and 0.0001%. It is clear that a 0.1% cutoff can cause positive or negative errors as large as 1%.

We summarize our principal conclusions.

(1) There are now available experimentally tested mathematical expressions for the Stokes drag on a circular cylinder in axial motion for the entire range of length to diameter ratio.

(2) When the known values of the ratio of transverse to axial drag for a cylinder are plotted versus ϵ, it is possible to connect these values with a smooth interpolation curve that allows the inference of approximate values of transverse drag from the known values of axial drag in the region $10 < L/D < 100$.

(3) The beads-on-a-shell method has been shown to give reliable drag values for a number of convex shapes, including bodies with sharp corners, but the stress force obtained from this method shows oscillations as a sharp corner is approached.

[1]J. Happel and H. Brenner, *Low Reynolds Number Hydrodynamics* (Nordhoff, Leyden, 1973), p. 341.
[2]G. K. Batchelor, *An Introduction to Fluid Dynamics* (Cambridge U. P., London, 1967), p. 195.
[3]J. M. Burgers, in *Second Report on Viscosity and Plasticity of the Amsterdam Academy of Sciences* (Nordemann, New York, 1938), Chap. 3.
[4]S. Broersma, J. Chem. Phys. **32**, 1632 (1960).
[5]R. G. Cox, J. Fluid Mech. **44**, 791 (1970).
[6]G. K. Batchelor, J. Fluid Mech. **44**, 419 (1970).
[7]J. B. Keller and S. I. Rubinow, J. Fluid Mech. **75**, 705 (1976).
[8]W. B. Russel, E. J. Hinch, L. G. Leal, and G. Tieffenbruck, J. Fluid Mech. **83**, 273 (1977).
[9]G. K. Youngren and A. Acrivos, J. Fluid Mech. **69**, 377 (1975).
[10]M. J. Gluckman, S. Weinbaum, and R. Pfeffer, J. Fluid Mech. **55**, 677 (1972).
[11]E. Swanson, D. Teller, and C. de Haen, J. Chem. Phys. **68**, 5097 (1978).
[12]J. F. Heiss and J. Coull, Chem. Eng. Prog. **48**, 133 (1952).
[13]P. N. Blumberg and C. M. Mohr, AIChe J. **14**, 331 (1968).
[14]N. J. de Mestre, J. Fluid Mech. **58**, 641 (1973).
[15]N. J. de Mestre and W. B. Russel, J. Eng. Math. **9**, 81 (1975).
[16]D. F. Moore, *Principles and Applications of Tribology* (Pergamon, New York, 1975), p. 113.
[17]A. M. D. Amarakoon, R. G. Hussey, B. J. Good, and E. G. Grimsal, Phys. Fluids **25**, 1495 (1982).
[18]D. R. Breach, J. Fluid Mech. **10**, 306 (1961).
[19]R. P. Roger and R. G. Hussey, Phys. Fluids **25**, 915 (1982).
[20]D. C. Teller, E. Swanson, and C. de Haen, in *Methods in Enzymology*, edited by C. H. W. Hirs (Academic, New York, 1979), Vol. 61, p. 112.
[21]J. Garcia de la Torre and V. A. Bloomfield, Q. Rev. Biophys. **14**, 81 (1981).
[22]I-D. Chang, Z. Angew. Math. Phys. **12**, 6 (1961).
[23]H. Brenner, J. Fluid Mech. **12**, 35 (1962).
[24]S. Wakiya, J. Phys. Soc. Jpn. **12**, 1130 (1957).
[25]W. E. Williams, J. Fluid Mech. **24**, 285 (1966).
[26]H. A. Oberbeck, Crelles J. **81**, 62 (1876).
[27]G. I. Tayor, in *Problems of Hydrodynamics and Continuum Mechanics* (SIAM, Philadelphia, 1969), English ed., p. 718; see also *Low Reynolds Number Flows* (film) (Educational Services, Cambridge, 1967).
[28]J. P. K. Tillett, J. Fluid Mech. **44**, 401 (1970).
[29]H. F. Weinberger, J. Fluid Mech. **52**, 321 (1972).
[30]J. F. Stalnaker and R. G. Hussey, Phys. Fluids **22**, 603 (1979).
[31]V. O'Brien, J. Fluids Eng. **104**, 500 (1982).
[32]S. Wakiya, Arch. Mech. **32**, 809 (1980).
[33]L. E. Payne and W. H. Pell, J. Fluid Mech. **7**, 529 (1960).
[34]S. Richardson, Q. J. Mech. Appl. Math. **30**, 369 (1977).
[35]D. H. Michael and M. E. O'Neill, J. Fluid Mech. **80**, 785 (1977).